Monthly Notices
of the
ROYAL ASTRONOMICAL SOCIETY

Mon. Not. R. Astron. Soc. **427,** 2275–2291 (2012) doi:10.1111/j.1365-2966.2012.22099.x

Heavily reddened quasars at $z \sim 2$ in the UKIDSS Large Area Survey: a transitional phase in AGN evolution

Manda Banerji,[1⋆] Richard G. McMahon,[1,2] Paul C. Hewett,[1] Susannah Alaghband-Zadeh,[1] Eduardo Gonzalez-Solares[1], Bram P. Venemans[3] and Melanie J. Hawthorn[1]

[1]*Institute of Astronomy, University of Cambridge, Madingley Road, Cambridge CB3 0HA*
[2]*Kavli Institute for Cosmology, University of Cambridge, Madingley Road, Cambridge CB3 0HA*
[3]*Max-Planck-Institut fur Astronomie, Konigstuhl 17, D-69117 Heidelberg, Germany*

Accepted 2012 September 10. Received 2012 September 10; in original form 2012 March 25

ABSTRACT

We present a new sample of purely near-infrared-selected $K_{\rm Vega} < 16.5$ [$K_{\rm AB} < 18.4$] extremely red [$(J - K)_{\rm Vega} > 2.5$] quasar candidates at $z \sim 2$ from $\simeq$900 deg^2 of data in the UKIDSS Large Area Survey (LAS). Five of these are spectroscopically confirmed to be heavily reddened type 1 active galactic nuclei (AGN) with broad emission lines bringing our total sample of reddened quasars from the UKIDSS-LAS to 12 at $z = 1.4$–2.7. At these redshifts, Hα (6563 Å) is in the K band. However, the mean Hα equivalent width of the reddened quasars is only 10 per cent larger than that of the optically selected population and cannot explain the extreme colours. Instead, dust extinction of $A_V \sim 2$–6 mag is required to reproduce the continuum colours of our sources. This is comparable to the dust extinctions seen in submillimetre galaxies at similar redshifts. We argue that the AGN are likely being observed in a relatively short-lived *breakout* phase when they are expelling gas and dust following a massive starburst, subsequently turning into UV-luminous quasars. Some of our quasars show direct evidence for strong outflows ($v \sim 800$–1000 km s^{-1}) affecting the Hα line consistent with this scenario. We predict that a larger fraction of reddened quasar hosts are likely to be submillimetre bright compared to the UV-luminous quasar population. We use our sample to place new constraints on the fraction of obscured type 1 AGN likely to be missed in optical surveys. Taken at face value our findings suggest that the obscured fraction depends on quasar luminosity. The space density of obscured quasars is approximately five times that inferred for UV-bright quasars from the Sloan Digital Sky Survey (SDSS) luminosity function at $M_i < -30$ but seems to drop at lower luminosities even accounting for various sources of incompleteness in our sample. We find that at $M_i \sim -28$ for example, this fraction is unlikely to be larger than $\sim$20 per cent although these fractions are highly uncertain at present due to the small size of our sample. A deeper K-band survey for highly obscured quasars is clearly needed to test this hypothesis fully and is now becoming possible with new sensitive all-sky infrared surveys such as the VISTA Hemisphere Survey and the *Wide Infrared Survey Explorer* (*WISE*) All Sky Survey.

Key words: galaxies: active – quasars: emission lines – quasars: general – quasars: individual.

1 INTRODUCTION

The past few years have seen an explosion in multi-wavelength surveys covering very large areas of sky and extending to wavelengths from the X-ray through the optical/infrared and into the submillimetre, millimetre and radio. Such surveys are not only allowing us to gain a more holistic view of galaxy and active galactic nuclei (AGN) properties by sampling their entire spectral energy distribution (SED), but their unprecedented area also opens up discovery space for rare and unusual classes of objects e.g. the most distant (Mortlock et al. 2011) as well as the most luminous quasars (Irwin et al. 1998). Observational studies of distant quasars and galaxies have gained new impetus recently with the advent of sensitive infrared detectors which are allowing us to observe the SEDs of galaxies and quasars after they have been redshifted beyond optical wavelengths. In addition to sources which appear red due to their

⋆E-mail: mbanerji@ast.cam.ac.uk

high redshifts, there is also a population of red sources where the red colours can be attributed to: an intrinsically red continuum; significant dust extinction associated with the quasar host galaxy; the presence of broad absorption lines (BAL); or a gravitationally lensed system where the foreground lensing galaxy and/or intervening absorption system redden the light (Gregg et al. 2002; Lacy et al. 2002). Long wavelengths such as the far-infrared and submillimetre have for some time been used to track very red, dust-enshrouded populations of galaxies (Blain et al. 2002; Smail et al. 2002) that are otherwise obscured in the optical. Now, the emergence of very Large Area Surveys (LAS) in the near- and mid-infrared wavelengths, such as the UKIRT Infrared Deep Sky Survey (UKIDSS) LAS (Lawrence et al. 2007), Visible and Infrared Survey Telescope for Astronomy (VISTA) Hemisphere Survey (VHS; McMahon et al., in preparation) and *Wide Infrared Survey Explorer* (*WISE*; Wright et al. 2010), is providing a different perspective on studies of red populations of galaxies and quasars. While these surveys are relatively shallow, the huge area of sky surveyed allows the detection of rare, luminous sources.

Quasar selection in large surveys has typically relied on detecting their excess in flux relative to stars at short UV wavelengths (Richards et al. 2002). However, quasars also display an infrared excess in the *K* band (Warren, Hewett & Foltz 2000) which allows the detection of a complementary sample of infrared bright sources that are relatively faint at optical wavelengths (Maddox et al. 2008). Although numerous attempts have previously been made at studying the infrared bright quasar population, the prevalence of Galactic stars with very similar colours to red quasars in near-infrared (NIR) surveys has meant that the selection of these objects has typically had to rely on optical-NIR colour cuts (Maddox et al. 2008) or matching to radio surveys (Glikman et al. 2007). A consequence of the heterogenous selection criteria used to isolate red quasars is that the exact fraction of obscured quasars, that are not detected in optical surveys, remains unclear. The estimates currently range from <20 per cent (Richards et al. 2003; Maddox et al. 2008) to 60 per cent (Glikman et al. 2007). As dust-obscured quasars are expected to be bright at NIR wavelengths, a homogenous flux-limited sample selected in the NIR allows one to estimate their true space density without requiring matches to other multi-wavelength surveys which inevitably introduce additional selection biases on the sample.

In Hawthorn et al. (in preparation, hereafter Paper I), we introduce a technique for isolating stellar Extremely Red Objects (EROs) from large area NIR surveys using a $(J - K)$ colour selection. It is shown that, provided the artefacts that dominate colour-selected samples of extreme objects are well understood, selecting bright EROs with stellar morphologies could prove effective in assembling a homogenous population of infrared-selected dusty type 1 AGN. Spectroscopic follow-up of 10 sources over $\sim$100 deg^2 in Paper I has led to the confirmation that seven are extremely red type 1 AGN with similar Hα equivalent widths to samples selected in the optical. The red colours in these quasars imply dust extinction values of $A_V \sim 2.3$.

In the current work, we present new spectra from a search for stellar EROs over a larger area using the same techniques as in Paper I. Taking the samples from both papers, we focus on the inferred properties of our infrared bright type 1 AGN and compare them to quasars selected at other wavelengths, from the optical to the submillimetre. Sanders et al. (1988) were the first to postulate that submillimetre luminous galaxies (SMGs) and quasars are different observational manifestations of the same sources. Major-merger-induced starbursts appear as submillimetre galaxies and as the dust clears from the decaying starburst, the central nuclear region is revealed as an optically bright quasar. Red BAL quasars that are enshrouded by dust have also been studied e.g. by Egami et al. (1996) and hypothesized to correspond to a young phase in quasar evolution. A sample of NIR-selected red quasars may therefore provide crucial observational evidence for the link between galaxies and supermassive black holes, representing a short-lived phase in the evolution of the galaxy where the dust has not yet fully cleared and is still obscuring the view of the quasar in the optical wavelengths.

Throughout this paper we assume a flat concordance cosmology with $H_0 = 70\,\mathrm{km\,s^{-1}\,Mpc^{-1}}$, $\Omega_\mathrm{M} = 0.3$ and $\Omega_\Lambda = 0.7$. All magnitudes quoted are in the native system of the survey being discussed – i.e. *AB* for Sloan Digital Sky Survey (SDSS) and Vega for UKIDSS unless otherwise stated. The *AB*-Vega conversions for both the SDSS and UKIDSS filters can be found in Hewett et al. (2006).

2 DATA

Red quasar candidates are selected from the UKIDSS LAS, one of the largest NIR surveys and the NIR counterpart to the SDSS in the Northern hemisphere. In Paper I, we have presented details of our candidate selection algorithm including how to effectively screen the data for the many spurious sources. Below, we provide a brief overview of some of the key features of our selection but the interested reader is referred to Paper I for more information.

2.1 Photometric selection

Red quasar candidates were selected from the UKIDSS-LAS data release 4 (DR4) by isolating sources with stellar morphologies and $J - K_\mathrm{Vega} > 2.5$ ($J - K_{AB} > 1.5$) and $K_\mathrm{Vega} < 16.5$ ($K_{AB} < 18.4$). They belong to a class of sources known as EROs. The UKIDSS-LAS DR4 footprint is shown in Fig. 1. Two samples were defined: (1) $08\,h <$ RA $<$ 16 h and $0^\circ <$ Dec. $< 15^\circ$ where we require a non-detection in the optical SDSS bands in order for the source to be included in our spectroscopic sample, and (2) the SDSS southern stripe: Stripe82 region at $21\,h <$ RA $<$ 00 h and $-1\overset{\circ}{.}25 <$ Dec. $< 1\overset{\circ}{.}25$ which benefits from deep co-added optical data (Annis et al. 2011). In the case of the Stripe82 sample, we use the deep co-add images to select sources that are fainter than $i_{AB} = 20.5$ and redder than $(i - K)_{AB} = 2.5$ [$(i - K)_\mathrm{Vega} = 4.4$] as was the case for the North Galactic Pole (NGP) part of the Stripe82 sample presented in Paper I. We also include four sources that are brighter than this *i*-band limit in order to check whether there are any reddened AGN that could potentially be missed by applying the SDSS *i*-band selection. Finally, to assess the utility of X-ray detections for identifying red, luminous AGNs, two objects included in the *2XMM* X-ray catalogue (Watson et al. 2009) that satisfy $K_\mathrm{Vega} < 17.0$ ($K_{AB} < 18.9$) were also targeted. The objects are the two brightest EROs that are known X-ray sources in the survey area.

The full area spanned by Sample 1 is 770 deg^2, calculated using the publicly available MANGLE software (Swanson et al. 2008). There are 43 EROs with $K_\mathrm{Vega} < 16.5$ and $(J - K)_\mathrm{Vega} > 2.5$. Nine of the 43 sources are undetected in the SDSS and therefore are candidate reddened type 1 AGN. In addition, ULAS J0908+1042 was targeted despite being detected in the SDSS as it is also a FIRST radio source. Finally, ULAS J1002+0137 was also targeted despite being fainter in *K* as it is an X-ray source. Sample 1 therefore comprises 11 red quasar candidates which are summarized in Table 1.

The South Galactic Pole (SGP) part of Sample 2 that overlaps the SDSS Stripe82 spans an additional 100 deg^2. There are 14 EROs in this area with $K(\mathrm{Vega}) < 16.5$ and $(J - K)_\mathrm{Vega} > 2.5$. Only three

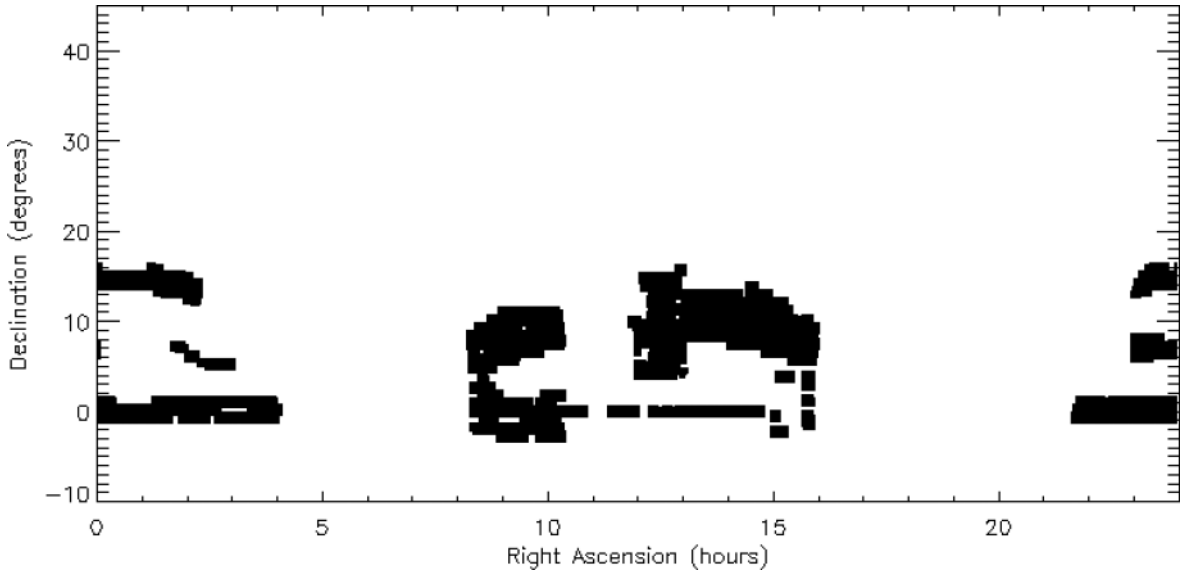

Figure 1. The UKIDSS-LAS DR4 footprint from which all targets in this paper have been selected.

Table 1. Sample of red quasar candidates from the UKIDSS-LAS DR4. Two samples are constructed at 08 h < RA < 16 h and overlapping the SGP part of the SDSS southern stripe: Stripe82. Slightly different selection criteria were used to select sources in these two samples as detailed in Section 2.1. Both sources that were spectroscopically followed-up using SINFONI as well as sources with no spectra are included for completeness. The NGP part of the Stripe82 sample was presented in Paper I as well as two of the quasars in Sample 1 that overlap the UKIDSS-LAS Early Data Release area.

Name	RA	Dec.	$K_{\rm Vega}$	i_{AB}	Redshift	Notes
Sample 1 08 H < RA < 16 H – 11 objects						
ULAS J0908+1042	09:08:06.81	+10:42:39.5	15.13	21.00	–	FIRST radio source
ULAS J0946+0016	09:46:28.66	+00:16:25.8	16.28	–	No spectrum	
ULAS J1002+0137[a]	10:02:11.29	+01:37:06.8	17.00	–	1.595	Faint *K*-band, *2XMM* X-ray source
ULAS J1004+0026	10:04:43.68	+00:26:09.8	15.51	–	–	
ULAS J1200+0423	12:00:59.45	+04:23:38.4	16.30	–	No spectrum	
ULAS J1234+0907	12:34:27.52	+09:07:54.2	16.15	–	2.503	
ULAS J1319+0009	13:19:10.66	+00:09:56.1	16.04	–	–	UKIDSS-EDR Paper I
ULAS J1320+0948	13:20:47.95	+09:08:05.8	16.46	–	No spectrum	
ULAS J1422+1023	14:22:39.13	+10:23:34.2	16.46	–	–	FIRST radio source
ULAS J1455+1230	14:55:21.00	+12:30:08.6	16.34	–	1.460	
ULAS J1539+0557	15:39:10.16	+05:57:49.7	15.85	–	2.658	UKIDSS-EDR Paper I
Sample 2 Stripe82 SGP 21 H < RA < 24 H – 8 objects						
ULAS J2148−0011	21:48:25.35	−00:11:32.1	15.49	20.41	–	Bright SDSS
ULAS J2150−0055	21:50:48.27	−00:55:45.8	15.13	20.53	–	On SDSS selection limit
ULAS J2200+0056	22:00:24.87	+00:56:04.8	15.22	21.00	2.541	Faint SDSS
ULAS J2219+0036	22:19:30.44	+00:36:26.4	15.61	19.06	–	Bright SDSS
ULAS J2224−0015	22:24:09.41	−00:15:24.1	16.07	21.77	2.223	Faint SDSS
ULAS J2251+0047	22:51:21.84	+00:47:33.4	15.65	20.08	–	Bright SDSS
ULAS J2343+0017	23:43:39.68	+00:17:56.0	16.68	22.00	–	Faint *K*-band, *2XMM* X-ray source
ULAS J2346−0038	23:46:58.41	−00:38:06.4	15.31	21.60	No spectrum	Faint SDSS

[a] COSMOS AGN.

of these are significantly fainter than $i = 20.5$ in the deeper SDSS co-add images and redder than $(i - K)_{AB} = 2.5$. Two of these, ULAS J2200+0056 and ULAS J2224−0015, were targeted for spectroscopy but the third, ULAS J2346−0038, was unfortunately incorrectly excluded from the spectroscopic target list as it had a close neighbour in a different frame set and was erroneously assumed to be a duplicate source. In addition, four other bright sources with $K_{\rm Vega} < 16$ that have $i_{AB} \leq 20.5$ were followed-up in order to assess whether any luminous *K*-band sources that are also detected in SDSS could potentially be reddened type 1 AGN. Finally, the fainter source ULAS J2343+0017 was also targeted on account of being detected in the X-ray. Therefore Sample 2 comprises eight potential red quasar candidates, four of which have $i \leq 20.5$.

In Table 1 we provide details of all our red quasar candidates in both samples including those without spectra. Fig. 2 shows the $(i - K)$ distribution of the EROs in Stripe82 with deep optical photometry. These include the SGP part of the sample presented in Table 1 of this paper as well as the NGP part of the sample presented in Paper I. We also plot several well-known red objects such as the dusty ultraluminous galaxies HR10 (Hu & Ridgway 1994; Dey et al. 1999) and IRAS F10214 (Rowan-Robinson et al.

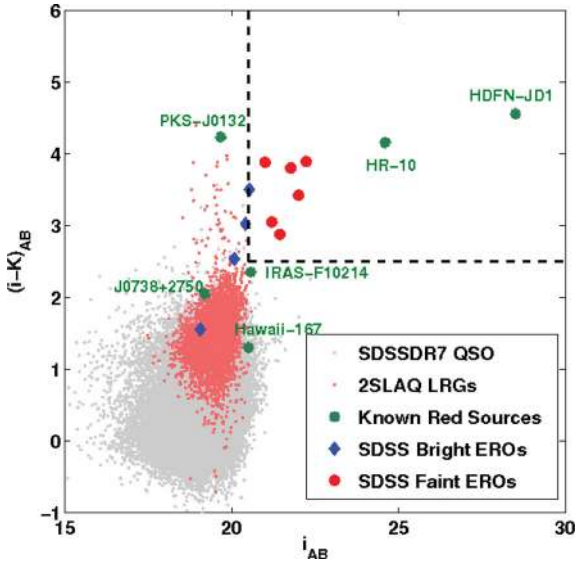

Figure 2. $i - K$ versus i_{AB} colour–magnitude diagram showing the EROs from our survey overlapping the deep SDSS Stripe82 co-add data. We also show the SDSS DR7 quasars (Schneider et al. 2010) as the grey points, Luminous Red Galaxies (LRGs) from the 2SLAQ survey (Cannon et al. 2006) as the small red points as well as various well-known red sources in green. Our selection criteria that divide SDSS-bright and faint EROs are shown by the dashed lines. The SDSS-bright EROs with $i < 20.5$ (blue) have no lines in the NIR spectra consistent with these being LRGs whereas the SDSS-faint EROs (red) are all spectroscopically confirmed to be reddened type 1 AGN.

1991), well-known red lensed quasars such as J0738+2750 and PKS−J0132 (Gregg et al. 2002) and red BAL quasars e.g. Hawaii-167 (Cowie et al. 1994; Egami et al. 1996). As can be seen from the figure, our ERO candidates are among the reddest infrared bright objects currently known. As discussed in detail in the next section, all the SDSS faint EROs are spectroscopically confirmed to be type 1 AGN whereas no redshifts were obtained for the SDSS bright EROs consistent with identifications as compact red galaxies.

2.2 Spectroscopic follow-up

Spectroscopic observations of our red quasar candidates were made with the SINFONI integral field spectrograph on the VLT (Eisenhauer et al. 2003; Bonnet et al. 2004) between 2009 April and July [Period83:383.A-0573(A)] with seeing ranging from 0.8 to 1.4 arcsec and the sample of 13 red quasar candidates that were observed is presented in Table 1. SINFONI was used in noAO mode with 0.25×0.25 arcsec^2 pixels corresponding to an 8×8 arcsec^2 field of view with the $R = 1500$ $H + K$ grism yielding a resolution of 12 Å or 185 km s^{-1} (measured from sky lines) and a dispersion of 5 Å per pixel. The observed wavelength range is 1.4–2.45 μm. The targets were offset by ±1.5 arcsec in RA and Dec. from the centre of the Integral Field Unit (IFU) for sky subtraction purposes, however always retaining the target in the field of view. The array centre therefore moved in a 3×3 arcsec^2. The data were reduced using standard SINFONI ESOREX pipelines which include extraction, sky subtraction, wavelength calibration and flat fielding.

All spectra were flux calibrated using standard telluric stars observed at similar airmass. The target spectrum is divided by the spectrum of the calibration star and multiplied by the appropriate blackbody, depending on the spectral type of the star, in order to get a relative flux-calibrated spectrum. Due to the absence of absolute spectrophotometric standards in the NIR, the relative flux-calibrated spectra are then normalized to the UKIDSS K-band magnitudes of the targets in order to provide an absolute flux calibration.

Three of the 13 quasar candidates observed show broad Hα emission in the K band and two have Hα emission in the H band. We fit multiple Gaussian components to the Hα line profile and redshifts are determined from the centroid of the intermediate component where present and from the centroid of the single Gaussian where only one component is required to fit the data. Redshifts are summarized in Table 1. In Fig. 3 we show spectra of the five new red quasars with redshifts as well as the seven confirmed quasars already presented in Paper I.

Out of the eight sources for which no redshifts were obtained, two have associated FIRST counterparts; so these could be lower redshift radio galaxies with compact morphologies. One of the X-ray sources is at the faint-end of our sample and below the nominal flux limit. However, the other X-ray source, ULAS J1002+0137, which also lies below the nominal flux limit of the survey, was spectroscopically confirmed to be a broad-line quasar at $z = 1.595$. This source is in the COSMOS field and therefore has ancillary multi-wavelength data. We discuss it in detail in Section 3.3.

In Sample 2, all the sources that had $i_{AB} > 20.5$ were spectroscopically confirmed to be reddened type 1 AGN. No redshifts were obtained for the four sources with $i_{AB} \leq 20.5$, consistent with these being compact elliptical galaxies. We note that three out of the four sources – ULAS J2148−0011, ULAS J2150−0055 and ULAS J2251+0047 – are indeed classified as galaxies in the SDSS imaging survey. We use the publicly available photometric redshift code EAZY (Brammer, van Dokkum & Coppi 2008) to calculate photometric redshifts for these four SDSS-bright EROs using an R-band luminosity function prior. The photometric redshifts of the four sources are summarized in Table 2.

The sources without redshifts which are also undetected in the optical filters could have several interpretations. The spectrum for the brightest of these, ULAS J1004+0026, is shown in Fig. 4 along with the sky transmission spectrum. If such unconfirmed candidates are quasars, as suggested by their compact morphologies and NIR colours, they may be at redshifts between 1.75 and 2.00 which corresponds to Hα lying in the region of strong atmospheric transmission between the H and K bands. Alternatively, there is a class of rare BAL quasars known as FeLOBALs (Voit, Weymann & Korista 1993; Becker et al. 1997, 2000; Hall et al. 2002) where strong absorption due to iron at relatively low ionization potentials means there is virtually no flux below $\lambda \sim 2800$ Å. It has been hypothesized that FeLOBALs may represent a transition population between ultra-luminous infrared galaxies (ULIRGs) and quasars with some of these sources having prodigiously high star formation rates, as inferred from their mid-infrared properties (Farrah et al. 2007). Although they are very rare, they would be preferentially selected in NIR-selected samples due to their very red colours – e.g. as in Urrutia et al. (2009). If some of our unidentified objects do indeed correspond to this class of objects, this would place them at $z \sim 3$–4 in order to reproduce the very red colours. This is consistent with the fraction of BALs increasing at these higher redshifts (Allen et al. 2011). Optical spectroscopy would help confirm the identity of these sources.

3 RESULTS

The spectra presented above combined with the sample in Paper I total 12 confirmed type 1 AGN with very red colours and redshifts

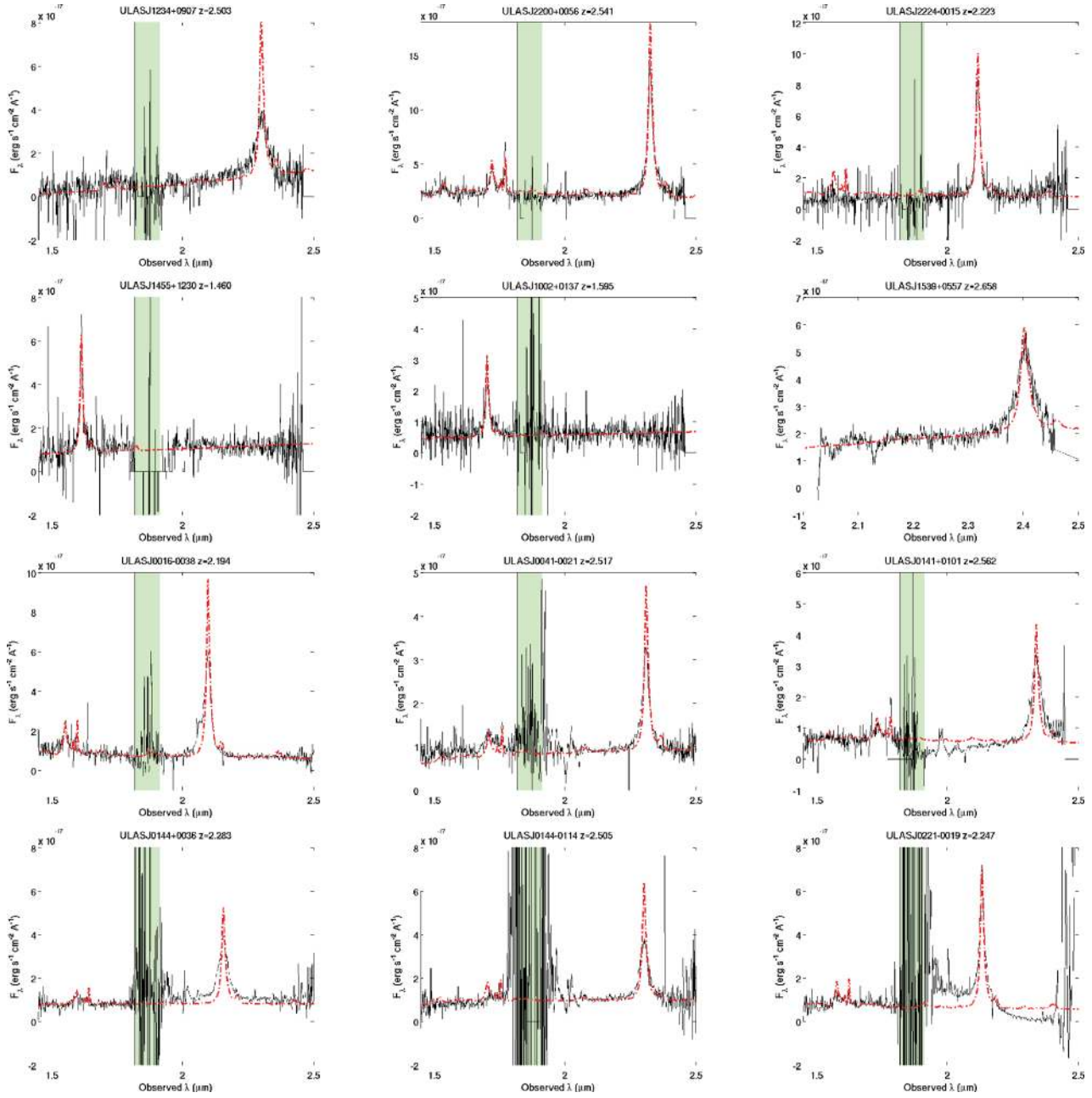

Figure 3. NIR spectra of all 12 confirmed reddened quasars with redshifts. The top two rows show VLT-SINFONI spectra apart from ULAS J1539+0557 which was observed using NIRSPEC on Keck. The bottom two rows show Gemini-GNIRS spectra. In the case of the GNIRS spectra, the *H*- and *K*-band orders are plotted together in these figures but problems with extracting the spectra at the edges of each order mean that the relative flux calibration between the two orders is unlikely to be accurate. All spectra have been smoothed by a three-pixel boxcar (0.0015 μm) for purposes of presentation. The red dot–dashed lines show the model fits derived for each quasar by fitting to the broad-band colours. The model SEDs are derived by fitting to the broad-band colours of the quasars with a simple scaling of Hα equivalent width to match the observations. The Hα line profiles in the models and observations are therefore not expected to match. The region of low atmospheric transmission between the *H* and *K* bands is shown as the grey rectangular area.

Table 2. Photometric redshifts for the four SDSS Stripe82 EROs with $i <= 20.5$ and for which no lines were identified in the NIR spectra.

Name	z_p
ULAS J2148−0011	$0.97 \pm {}^{0.08}_{0.09}$
ULAS J2150−0055	1.30 ± 0.08
ULAS J2219+0036	2.71 ± 0.06
ULAS J2251+0047	0.85 ± 0.05

between 1.4 and 2.7. We now turn to a detailed assessment of their properties.

3.1 Model SEDs

We begin by fitting model type 1 AGN SEDs to the available SDSS+UKIDSS broad-band photometry for all our quasars. The photometric data are chosen for the fitting as it covers a larger wavelength range than our NIR spectra and includes flux points at

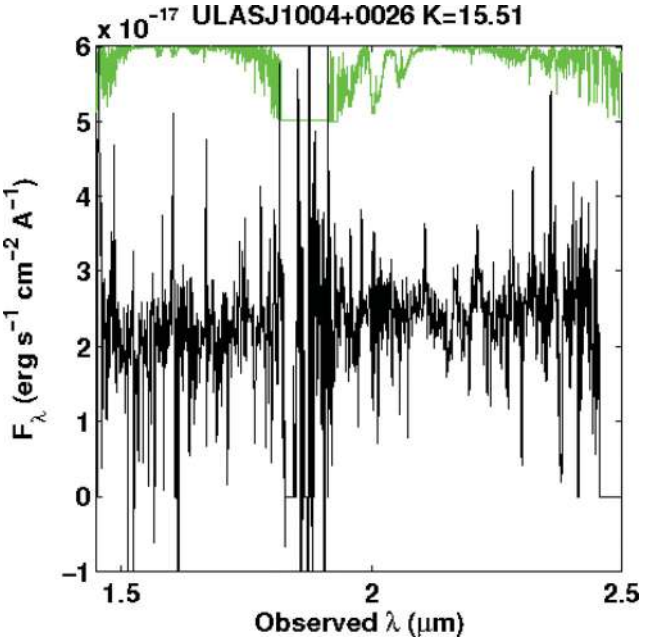

Figure 4. SINFONI spectrum of our brightest unconfirmed target ULAS J1004+0026 which is unlikely to be an elliptical or low-redshift radio galaxy. The atmospheric transmission spectrum from VLT-ISAAC is also shown for reference at the top of the panel and demonstrates the wavelength region (1.80–1.97 μm corresponding to Hα at $1.75 < z < 2$) where no lines can be observed due to atmospheric opacity.

bluer wavelengths which are more sensitive to dust extinction. The unreddened 'standard' quasar model is described in section 2.4 of Maddox et al. (2008). The model SED reproduces the SDSS *ugriz* and UKIDSS *YJHK* broad-band colours of the majority of quasars, selected in the SDSS, to high accuracy over the redshift range $0.2 \leq z \leq 5$. The aim of fitting these model SEDs to the quasar photometry is to infer the amount of dust extinction in each quasar from the observed colours. Although other factors such as lensing and variability may also contribute to the red colours, these are unlikely to be significant in our sample. All our quasars lie at $z \gtrsim 1.5$ and are very luminous so the host galaxy contribution to the broad-band light is likely to be insignificant. While variability can certainly affect the spectral shape of quasars, the effect is more pronounced in the rest-frame UV bands and lower luminosity objects (Hook et al. 1994) and more often seen in radio-loud populations (Helfand et al. 2001). Only two of our 12 quasars, ULAS J0016−0038 and ULAS J0141+0101, are radio-loud. We discuss the possibility of lensing in detail in Section 4.1 where we conclude that it is unlikely to affect the majority of our sample. We therefore proceed by assuming that the red NIR colours seen in our quasars are due to dust extinction.

Reddened model SEDs were therefore created for each quasar by including the effect of an extinction curve with a specified $E(B-V)$. The form of the extinction curve used is very similar to that of Gallerani et al. (2010) but in the rest-frame wavelength interval of interest here, 2500–10 000 Å, the differences between commonly used extinction curves (e.g. Large Magellanic Cloud, Small Magellanic Cloud and Milky Way) are small and the results are not dependent on the choice of extinction curve. The facility to adjust the emission line equivalent widths is also incorporated in the models and object-specific model SEDs were generated by matching the measured Hα equivalent widths. We stress, however, that we do not attempt to match the Hα line profiles in the model and observed spectra apart from this simple scaling of the equivalent widths. In this way, we can disentangle the effects of Hα equivalent width and dust extinction in the observed $(J-K)$ colours.

In a few cases, the $(J-K)$ and $(H-K)$ colours are marginally inconsistent with a single reddening value so we quote the best-fitting extinction values needed to reproduce each of the observed colours. However, the inferred $E(B-V)$ values are always similar and the conclusions of the paper do not depend critically on which values are adopted. For the rest of the paper, we use the extinction values derived by matching to the $(J-K)$ colours so as to provide a larger baseline in terms of wavelength for the extinction estimates. An $R_V = 3.1$, consistent with the dust in our own Milky Way, is assumed throughout.[1]

In Table 3 we quote the dust extinction, A_V inferred from the model fits for our combined sample of reddened quasars from Paper I and the current work. We also give the factor by which the Hα equivalent widths in the model is scaled in order to reproduce the observations. Previous studies by Glikman et al. (2007) did not account for the effect of the Hα equivalent widths on the $(J-K)$ colours. Fig. 3 shows these best-fitting model SEDs overlaid on the observed rest-frame optical spectra for all our spectroscopically confirmed red quasars. Note that the model fits were derived from the broad-band photometry only with a simple scaling adopted to match the observed Hα equivalent widths so the match between these model SEDs and the observed continuum flux in the spectra is, in most cases, very good. In some cases – e.g. ULAS J0221−0019 – the models do not match the continuum in the observed spectra at the edges of the spectral orders due to problems with extracting the spectra at the edges. We see from Table 3, however, that the match between the observed and model colours is always very good. The median difference in the model and observed $(H-K)$ colours is 0.005.

From Table 3 it can immediately be seen that most of the red quasars have similar Hα equivalent widths to the standard model spectrum constructed from the optically selected quasar population, with the strongest Hα line having an equivalent width of only a factor of 2 larger. However, we find that significant dust extinction is required to reproduce the continuum colours, with a mean dust extinction of $A_V \sim 2.5$ for all our sources. ULAS J1234+0907, our reddest object, has a dust extinction of $A_V = 6.0$ inferred from its $(H-K)$ colour and is one of the reddest quasars currently known.

3.2 Linewidths, bolometric luminosities and black hole masses

In this section, we assess the emission line properties of our 12 red quasars. In order to do so, we fit multiple Gaussian components to the Hα line profiles of all our quasars with spectroscopic redshifts after blueshifting to the rest frame. Note that these Gaussian fits to the observed Hα lines are distinct from the model SED fits done to the broad-band photometry in Section 3.1 to infer a dust extinction. The effect of this dust extinction on the full width half-maximum (FWHM) of the Hα line is expected to be very small. The Gaussian fits can be seen in Figs 5 and 6 for the new sample presented in this paper and the Paper I sample, respectively. The derived linewidths are summarized in Table 4. Errors are derived from a least-squares fit of the Gaussian profiles to the data. In most cases, both intermediate and broad components are needed to fit the line profiles adequately. The presence of a very broad Hα component with FWHM $> 5000\,\mathrm{km\,s^{-1}}$ in these quasars confirms that we are

[1] Considering possible variations in the dust law in distant quasars is beyond the scope of this work.

Table 3. Summary of model fits for spectroscopically confirmed red quasars.

Name	Redshift	$(J-K)_{\rm obs}$	$(J-K)_{\rm model}$	$(H-K)_{\rm obs}$	$(H-K)_{\rm model}$	A_V	Hα EW scaling
ULAS J0016−0038	2.194	1.607	1.702	0.871	0.882	1.7	2.1
ULAS J0041−0021	2.517	2.171	1.821	0.851	0.869	2.1	0.7
	2.517	2.171	2.167	0.851	1.023	2.5	0.7
ULAS J0141+0101	2.562	1.767	1.752	0.893	0.893	1.8	1.2
ULAS J0144−0114	2.505	1.852	1.852	1.009	0.897	2.1	1.0
	2.505	1.852	2.099	1.009	1.007	2.4	1.0
ULAS J0144+0036	2.283	1.902	1.496	0.726	0.734	1.7	0.9
	2.283	1.902	1.901	0.726	0.913	2.3	0.9
ULAS J0221−0019	2.247	–	1.690	0.854	0.856	1.8	1.6
ULAS J1539+0557	2.658	–	3.290	1.440	1.450	4.0	0.3
ULAS J1002+0137	1.595	–	1.657	0.551	0.550	3.2	0.8
ULAS J1234+0907	2.503	–	5.065	2.321	2.331	6.0	1.3
ULAS J1455+1230	1.460	2.212	1.729	0.570	0.571	3.4	0.9
	1.460	2.212	2.219	0.570	0.790	4.3	0.9
ULAS J2200+0056	2.541	1.693	1.617	0.798	0.815	1.7	1.3
ULAS J2224−0015	2.223	1.747	1.798	0.910	0.912	1.9	1.7

able to at least partially see through into the broad-line region located close to the black hole accretion disc. The broad components in our sample typically have FWHM $= 6000\,{\rm km\,s^{-1}}$ while the intermediate component has an average FWHM $= 2230\,{\rm km\,s^{-1}}$. Our red quasars are therefore likely to be canonical type 1 AGN rather than type 2 AGN that are obscured by a dusty torus (e.g. Martínez-Sansigre et al. 2005). In the latter case we would not be able to detect the broad component for most lines of sight. We conclude that the large dust extinction values must be arising in the host galaxy of the quasar rather than from the molecular torus.

The Hα line properties can be used to infer black hole masses, bolometric luminosities as well as Eddington fractions using the scaling relations between Hα and Hβ linewidth (Greene & Ho 2005) from reverberation mapping (Kaspi et al. 2007). We correct the line for the instrumental broadening of $185\,{\rm km\,s^{-1}}$ by subtracting this in quadrature from the observed linewidth and use the following equations:

$$\mathrm{FWHM_{H\beta}} = (1.07\pm0.07)\times10^3\left(\frac{\mathrm{FWHM_{H\alpha}}}{10^3\,\mathrm{km\,s^{-1}}}\right)^{1.03\pm0.03}\ \mathrm{km\,s^{-1}}. \quad (1)$$

The black hole mass is then determined from the Hβ FWHM using

$$M_{\rm BH}/{\rm M_\odot} = 10^{6.91}\left(\frac{\mathrm{FWHM_{H\beta}}}{1000\,\mathrm{km\,s^{-1}}}\right)^2\left(\frac{L_{5100}}{10^{44}\,\mathrm{erg\,s^{-1}}}\right)^{0.5}. \quad (2)$$

where L_{5100} is estimated using the best-fitting model SEDs of each quasar. We assume that the bolometric luminosity is given by $L_{\rm bol} = 7L_{5100}$ (Vestergaard & Peterson 2006) and use these to calculate the Eddington fraction. The mass accretion rate is given by

$$\frac{{\rm d}m}{{\rm d}t} = 0.18\frac{1}{\epsilon}\left(\frac{L_{\rm bol}}{10^{46}\,\mathrm{erg\,s^{-1}}}\right)\mathrm{M_\odot\,yr^{-1}}, \quad (3)$$

where the accretion efficiency, ϵ, is assumed to be 10 per cent and the factor of 0.18 results from the units being used in equation (3). The derived luminosities, masses, Eddington fractions and accretion rates are summarized in Table 5. The quoted errors are derived by propagating the fit errors to the Hα linewidths.

In addition to these fit errors, there are also systematic errors affecting the black hole mass estimates that should be discussed. We therefore highlight several caveats relevant to the black hole mass estimates in Table 5, which may result in large systematic uncertainties. In all cases, black hole masses were estimated using the FWHM of a single Gaussian fit to the Hα line profile. However, using the broad component only to estimate the black hole masses would result in an increase in the black hole masses and correspondingly a decrease in the Eddington fractions by up to a factor of ∼2. Furthermore, we note that several of our Gaussian line profiles in Figs 5 and 6 are highly asymmetric showing large velocity shifts between the different components.

3.2.1 Evidence for outflows

In most cases, the broad component shows a clear blueshift relative to the intermediate component. This blueshift is most pronounced in ULAS J0016−0038 and ULAS J0041−0021 where the broad component has a velocity of $-1400\,{\rm km\,s^{-1}}$ and $-800\,{\rm km\,s^{-1}}$ relative to the intermediate component in the two respective sources. In ULAS J1455+1230, however, the broad component is redshifted by $+760\,{\rm km\,s^{-1}}$ relative to the intermediate component. Outflowing material in a bipolar flow can produce both blue- and redshifted emission so these velocity shifts indicate the presence of strong outflows that are affecting the broad-line region of the quasar. Signatures of outflows, while not generally seen in the UV-luminous quasar population, are not uncommon in samples of red BAL quasars where they have been shown to quench star formation within their host galaxies (Farrah et al. 2012). These flows can broaden the Hα linewidths leading to an overestimation of the virial black hole masses and consequently an underestimate of the Eddington fractions. We do not correct for this effect in our black hole mass estimates but caution that excluding the blue/red asymmetric component from the Hα line fits in quasars showing evidence for outflows results in a decrease in the estimated black hole masses by a factor of ∼2–3.

3.3 Notes on individual sources

Two of the sources in our reddened AGN sample are particularly interesting and merit further discussion.

ULAS J1234+0907: ULAS J1234+0907 is our reddest quasar with $(H-K) = 2.3$ and an inferred dust extinction of $A_V = 6.0$ derived from this colour. The extinction-corrected bolometric luminosity for this source is $L_{\rm bol} > 10^{48}{\rm erg\ s^{-1}}$ and the inferred black hole mass is $>10^{10}\,{\rm M_\odot}$ from the very broad Hα line seen in Fig. 3. This makes ULAS J1234+0907 one of the most bolometrically luminous and massive black holes known at $z \sim 2$. As discussed in

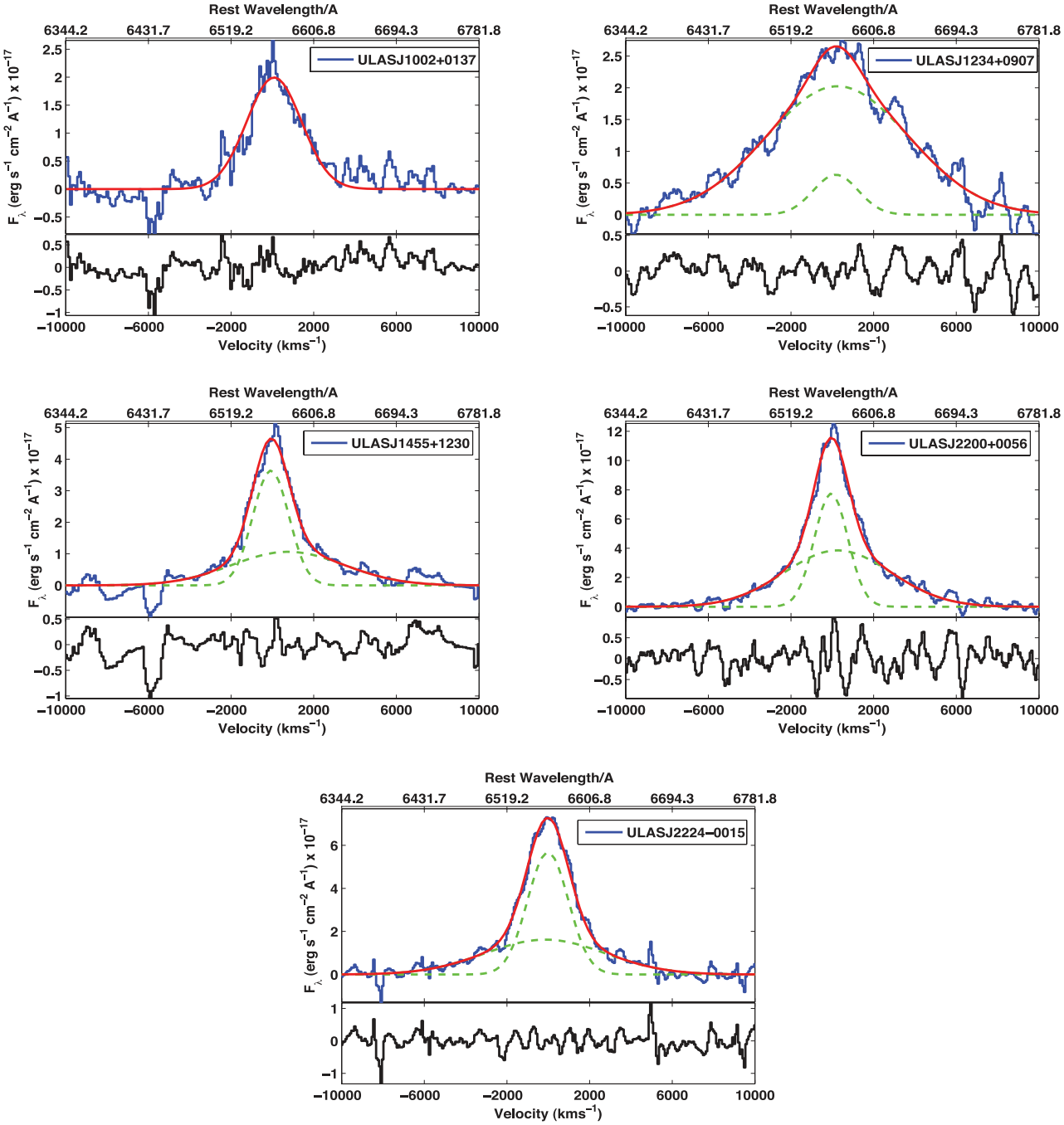

Figure 5. Gaussian fits to Hα line for the five new quasars. All observed spectra have been smoothed by a five-pixel boxcar for purposes of presentation. A broad and an intermediate component are needed to fit the line profiles adequately for most of the sources. These individual components are shown as the dashed lines whereas the solid lines show the sum of the two components. We note that in the case of ULAS J1002+0137 a single-component fit, with FWHM $= 3200 \pm 300\,\mathrm{km\,s^{-1}}$, produced an equally good χ^2. The residuals from the fits are also shown at the bottom of each panel.

detail in Section 4, the extinction-corrected absolute magnitude for ULAS J1234+0907 is $M_i \sim -31$ to -32 which is comparable to the known lensed reddened quasar PKS 0132 at similar redshifts (Hall et al. 2002; Gregg et al. 2002). Our ongoing follow-up observations of ULAS J1234+0907 at long wavelengths will enable a detailed characterization of its host galaxy properties, shedding light on the reason for the extreme luminosity and dust extinction. Although we cannot exclude lensing as a possible reason for the extreme luminosity of this source we discuss why this is statistically improbable in Section 4.1.

ULAS J1002+0137: ULAS J1002+0137 is in the COSMOS field and has previously been studied by Mainieri et al. (2007) in their analysis of X-ray AGN from the *XMM–Newton* Wide Field Survey. The optical counterpart to the X-ray source is presented in Brusa et al. (2010). Although a redshift of $z = 0.784$ was initially derived by Mainieri et al. (2007) and Trump et al. (2009), the optical spectroscopic redshift of $z = 1.592$ in Brusa et al. (2010) agrees well with our Hα redshift and the photometric redshift of Salvato et al. (2009). The X-ray spectrum is best fitted by an absorbed power law and an Fe Kα line at $z = 0.784$. The multi-wavelength analysis and optical

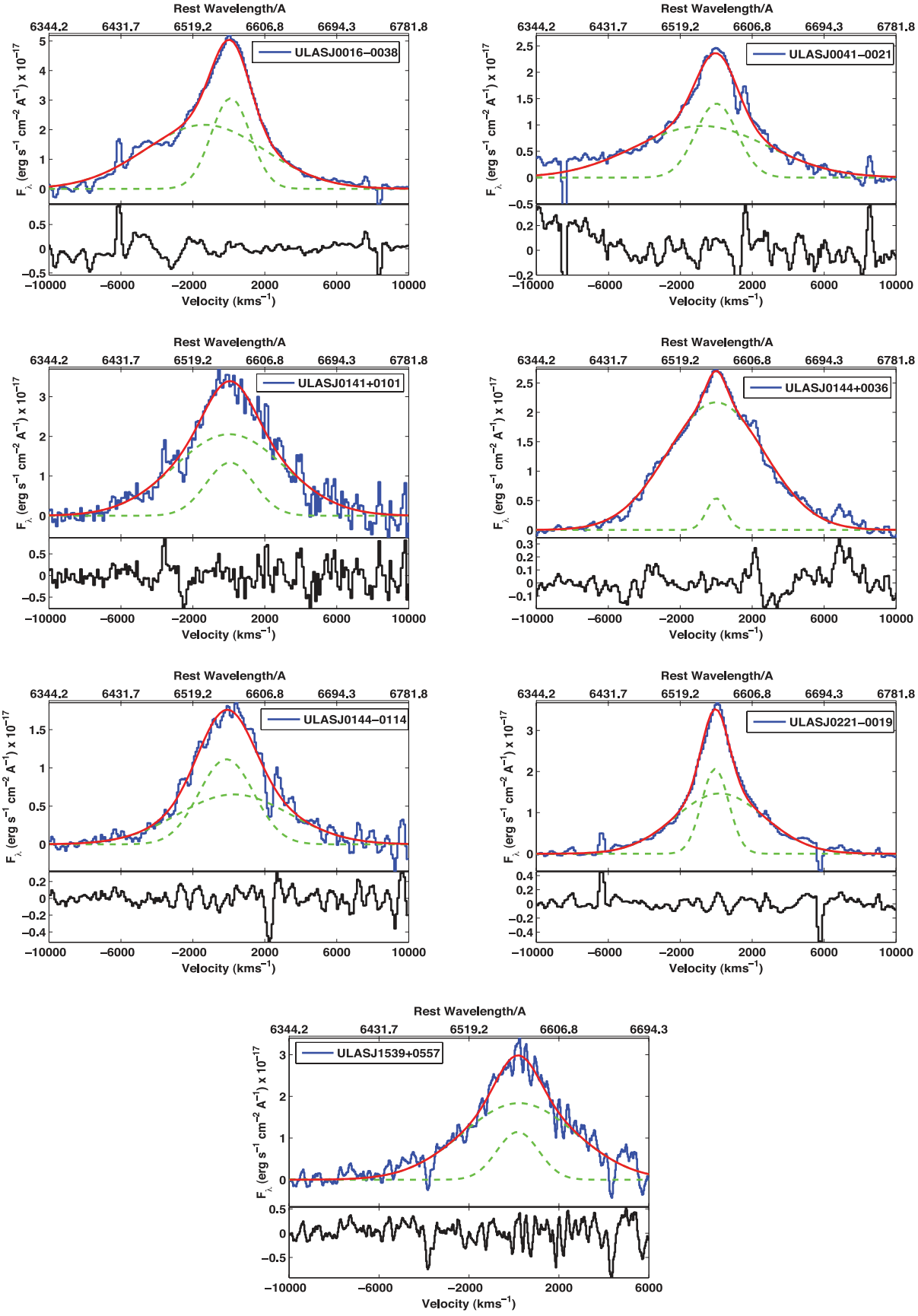

Figure 6. As in Fig. 5 but for the Paper I sample.

Table 4. Hα FWHM derived by fitting both a single Gaussian and two (broad and an intermediate components) Gaussian to the Hα line profiles. A narrow Hα component was not required in any of the sources.

Name	$\mathrm{FWHM}^{\mathrm{single}}_{\mathrm{H}\alpha}$/km s^{-1}	$\mathrm{FWHM}^{\mathrm{broad}}_{\mathrm{H}\alpha}$/km s^{-1}	$\mathrm{FWHM}^{\mathrm{int}}_{\mathrm{H}\alpha}$/km s^{-1}
ULAS J0016−0038	5400 ± 400	7900 ± 200	2620 ± 70
ULAS J0041−0021	5500 ± 500	8700 ± 600	2800 ± 200
ULAS J0141+0101	5900 ± 300	7300 ± 300	3200 ± 100
ULAS J0144+0036	6000 ± 200	6400 ± 200	1410 ± 40
ULAS J0144−0114	4700 ± 400	5400 ± 500	2800 ± 200
ULAS J0221−0019	3700 ± 200	6000 ± 100	1950 ± 30
ULAS J1539+0557	4700 ± 400	5900 ± 400	2200 ± 200
ULAS J1002+0137	3200 ± 300	–	–
ULAS J1234+0907	7300 ± 600	8100 ± 600	2600 ± 200
ULAS J1455+1230	2900 ± 200	6400 ± 300	2000 ± 100
ULAS J2200+0056	3300 ± 200	6200 ± 100	1960 ± 40
ULAS J2224−0015	3100 ± 100	6700 ± 200	2350 ± 60

Table 5. Bolometric luminosities, virial black hole masses, Eddington fractions and mass accretion rates derived for the 12 reddened quasars.

Name	$\log_{10}(L_{\mathrm{bol}}/\mathrm{erg\ s^{-1}})$	$\log_{10}(M_{\mathrm{BH}}/\mathrm{M}_{\odot})$	$L_{\mathrm{bol}}/L_{\mathrm{Edd}}$	dm/dt ($\mathrm{M}_{\odot}$ yr^{-1})
ULAS J0016−0038	46.9	9.32 ± 0.06	0.20 ± 0.05	13
ULAS J0041−0021	47.3	9.56 ± 0.08	0.30 ± 0.01	37
ULAS J0141+0101	46.9	9.41 ± 0.04	0.17 ± 0.02	14
ULAS J0144−0114	47.3	9.47 ± 0.07	0.37 ± 0.02	36
ULAS J0144+0036	47.1	9.53 ± 0.03	0.19 ± 0.01	22
ULAS J0221−0019	46.8	8.96 ± 0.05	0.40 ± 0.02	12
ULAS J1539+0557	48.2	9.87 ± 0.07	1.07 ± 0.06	264
ULAS J1002+0137	46.8	8.83 ± 0.08	0.50 ± 0.03	11
ULAS J1234+0907	48.5	10.43 ± 0.07	0.65 ± 0.04	580
ULAS J1455+1230	47.2	8.94 ± 0.06	1.04 ± 0.05	30
ULAS J2200+0056	47.4	9.18 ± 0.05	0.99 ± 0.04	50
ULAS J2224−0015	47.0	8.93 ± 0.03	0.68 ± 0.02	19

spectroscopy produce a classification as a narrow-line/type 2 AGN (Brusa et al. 2010). Our measured Hα FWHM of $\simeq$3000 km s^{-1} would suggest that the broad-line region is at least partially visible. However, this FWHM is significantly smaller than the broad components for the rest of the sample and ULAS J1002+0137 is the only source where a single Gaussian provides an adequate fit. If the broad-line region is partially obscured by a dusty torus, the large dust extinction of $A_V = 3.2$ inferred for this source would mean that the broad-line flux is expected to be more suppressed in the rest-frame ultraviolet than in the optical. This may have prevented this source from being classified as a broad-line AGN from the optical spectrum.

We should also consider the possibility that this is a lensed quasar with the source at $z = 1.595$ and the lens at $z = 0.784$. In Fig. 7 we show a 15 × 15 arcsec^2 COSMOS *BiK* composite around the source at a resolution of 0.15 arcsec per pixel (McCracken et al. 2010). An excess of blue sources is seen around the red quasar and the three blue sources to the southwest of ULAS J1002+0137 could be a lensed arc although the suggestion is highly tentative. We discuss the possibility of lensing in our sample further in Section 4.1.

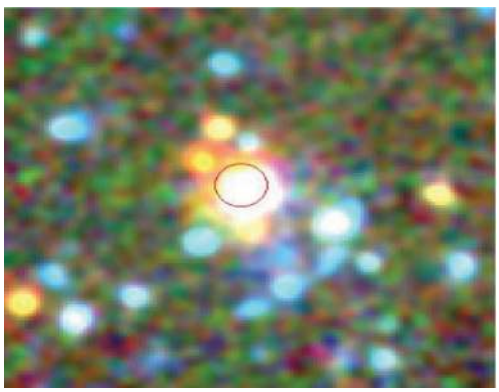

Figure 7. COSMOS *B*, *i*, *K* composite 15 × 15 arcsec^2 cut-out around ULAS J1002+0137. The quasar is marked with the circle. An excess of blue galaxies is seen around the source and the three sources located southwest of the quasar could be a lensed arc.

4 DISCUSSION

4.1 Lensing in the reddened quasar population

It has previously been demonstrated that lensing may be responsible for reddening the optical and infrared colours of quasars (Malhotra, Rhoads & Turner 1997). There are various explanations for why this may be the case. First, dust from a lens galaxy could extinct the light coming from the quasar as in the case of the lensed quasar PKS 1830−211 (Courbin et al. 1998). Alternatively, there could be a contribution to the quasar colours from galactic starlight within the lensing galaxy. There are various examples of lensed quasars in the literature which were selected based on their infrared excess. These include J0134−0931 otherwise known as PKS 0132 (Gregg et al.

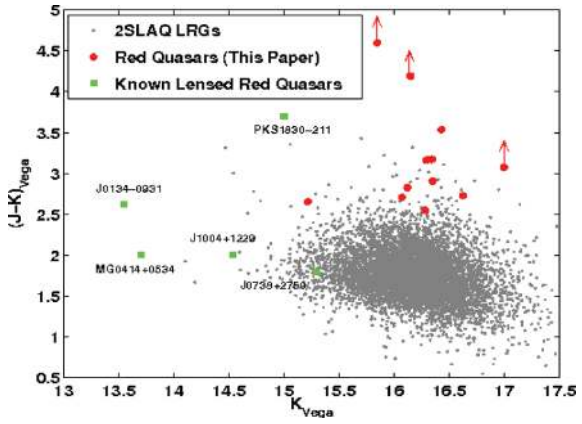

Figure 8. ($J - K$) versus K(Vega) colour–magnitude diagram comparing our sample of reddened quasars to some well-known lensed reddened quasars at similar redshifts as well as lower redshift LRGs, representative of the likely lens. Our sample of reddened quasars is always fainter and almost always redder than the known lensed reddened quasars and significantly redder than the LRG lenses.

2002; Hall et al. 2002; Winn et al. 2002), FIRST J1004+1229 (Lacy et al. 2002) and SDSS J1313+5151 (Ofek et al. 2007). In Fig. 8, we compare the colours and magnitudes of our reddened quasars to some of these known lensed quasars, selected based on their infrared excess. In the same plot we also show the distribution of LRGs from the 2SLAQ survey at $0.4 < z < 0.8$ (Cannon et al. 2006) which have been matched to the UKIDSS-LAS using a matching radius of 1.5 arcsec. These LRGs may be considered to be representative of the likely lens population.

In the previous section we presented some very tentative evidence for ULAS J1002+0137 being a lensed object based on the two different redshifts measured and the excess of blue galaxies in the deep COSMOS images. It is interesting to consider the likelihood of lensing in our population of NIR-selected red quasars. Based on Fig. 8 it can be seen that our reddened quasars are both apparently fainter and redder in colour than most of the known lensed red quasars. PKS 1830−211 has a very red observed colour on account of lying in the Galactic plane but this is not generally true of the other lensed objects. Lensing galaxies are typically LRGs at $z < 1$ in which case they should be detectable in the SDSS i and z bands as well as the bluer UKIDSS bands. The reddened quasars that are undetected in the SDSS as well as the UKIDSS Y and J bands include our reddest and intrinsically brightest source ULAS J1234+0907. Even if the lensing galaxy had a redshift as high as $z \simeq 1$, we would expect to be able to detect it in the UKIDSS Y and J bands.

We conclude that although we cannot rule out the possibility of some of the reddened quasars in our sample being lensed, in general this is unlikely to be the case for the bulk of the population and dust extinction within the quasar host is a more plausible explanation for the extreme colours observed in these sources.

4.2 Reddened quasars: a transition population between the starburst and optical AGN phases?

Our study of extremely red NIR-selected bright quasars has unearthed a population of broad-line AGN at $z \sim 2$ corresponding to the main epoch of galaxy formation with significant dust extinction of $A_V \gtrsim 2$ mag and comparable to that measured in the submillimetre galaxy population (Takata et al. 2006). We have already ruled out lensing as a possible explanation for the extreme colours in the bulk of this population. The very large observed widths (∼5000 km s^{-1}) of the Balmer emission lines support the hypothesis that the reddening is produced by dust within the host galaxy rather than a molecular torus which would obscure our view of the AGN broad-line region. An explanation that does not rely on viewing orientation is supported by the fact that the bolometric luminosities are typically very high and comparable to some of the most luminous optically selected quasars. The inferred mass accretion rates are therefore also high. The fuel for this black hole accretion likely comes from intense star formation within the host galaxy, consistent with the high dust extinctions being produced by a major starburst event. Highly star-forming, dust-obscured, ULIRGs and quasars are thought to be different observational manifestations of the same phenomena (Sanders et al. 1988). Major-merger-induced starbursts appear as ULIRGs or SMGs at $z \sim 2$ (Blain et al. 2002; Smail et al. 2002) and as the dust clears from the decaying starburst, the central nuclear region is revealed as an optically bright quasar. Our sample of infrared bright reddened quasars may therefore represent a transition phase between the starburst and optical quasar phases where the dust has not yet fully cleared, preventing the sources from being selected as ultraviolet-luminous quasars. This *blowout* phase is also evidenced by the presence of strong outflows that seem to be affecting the Hα line profiles in some of our quasars.

We now compare our sample properties to those of AGN samples selected at other wavelengths. These include the optically selected quasar population from SDSS DR7 (Shen et al. 2011), submillimetre bright quasars from Coppin et al. (2008) and Orellana et al. (2011), and a subset of submillimetre galaxies hosting AGN that were selected from X-ray studies (Alexander et al. 2008). The submillimetre quasars in Orellana et al. (2011) are all optically bright blue quasars whereas those in Coppin et al. (2008) include both standard blue optical quasars as well as redder X-ray absorbed quasars and quasars detected in blank-field submillimetre surveys. In Fig. 9 we plot the black hole masses as a function of redshift as well as bolometric luminosity for all these samples. The AGN bolometric luminosity for the SMGs was estimated by scaling the X-ray luminosities by a factor of 35 (Alexander et al. 2008). Note that the scaling relations we use implicitly assume that the black hole mass correlates with the bolometric luminosity so the trend seen in Fig. 9 should be interpreted with caution.

Fig. 9 shows that our sample of reddened quasars constitute some of the most massive AGN at $z \sim 2$ with black hole masses comparable to the quasars studied by Coppin et al. (2008) and Orellana et al. (2011) and an order of magnitude larger than SMGs hosting AGN at similar redshifts. We note in particular that the most massive black holes in the Coppin et al. (2008) sample are the optically bright subset of their population and the X-ray absorbed and submillimetre detected sources in their sample have relatively modest black hole masses. Our quasars are therefore as massive as the most luminous optically selected quasars but still have significant amounts of dust. These results are consistent with a scenario where the growth of the black hole follows the starburst phase. In other words, the quasars found in blank submillimetre surveys and the SMGs hosting AGN have not yet had time to significantly grow their black holes and represent an earlier evolutionary stage in the lifecycle of these sources.

Recently, Hickox et al. (2012) used clustering arguments to provide indirect evidence that powerful starbursts and optical quasars occur in the same systems. Our ongoing follow-up of the reddened quasars at submillimetre wavelengths would provide direct evidence for this link between starbursts and AGN. If the reddened quasars are indeed transitioning from starbursts to UV-bright quasars, the

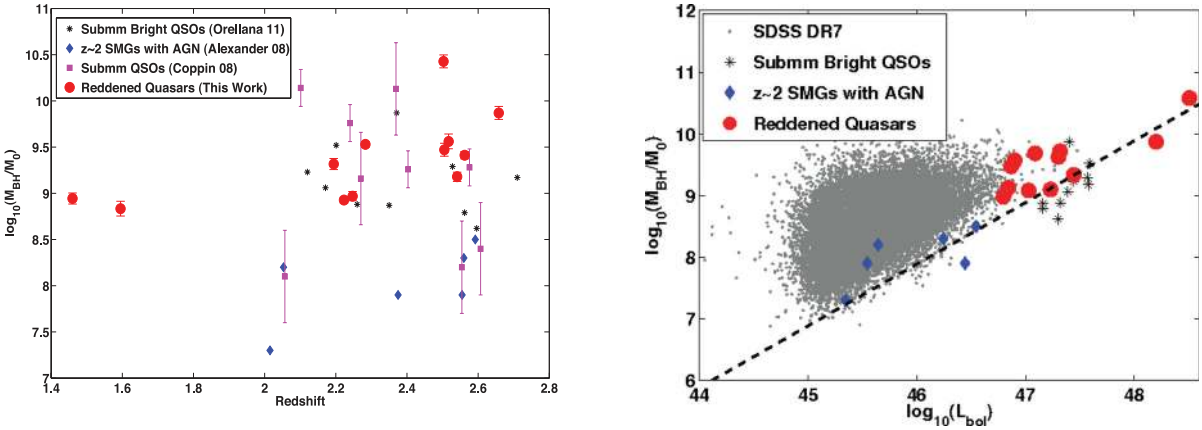

Figure 9. Left: redshift versus black hole mass of our reddened quasars compared to submillimetre bright quasars from Coppin et al. (2008) and Orellana et al. (2011) as well as X-ray-selected submillimetre galaxies hosting AGN from Alexander et al. (2008). Our sample of reddened quasars constitutes some of the most massive black holes at $z \sim 2$. Right: bolometric luminosity versus black hole mass for our sample of reddened quasars compared to the optically selected quasars from the SDSS (Shen et al. 2011), submillimetre bright quasars (Orellana et al. 2011) and submillimetre galaxies hosting AGN (Alexander et al. 2008). The dashed line corresponds to Eddington accretion. Note that the scaling relations used to derive the black hole masses and bolometric luminosities means the two quantities are necessarily correlated.

expectation is that the host galaxies of our population are likely to be more luminous at far-infrared and submillimetre wavelengths than the hosts of the optical QSO population (e.g. Isaak et al. 2002; Priddey et al. 2003). If we assume that most of the mass in quasars is assembled at $z \geq 2$ (McLure & Dunlop 2004) consistent with *downsizing* in the quasar population, then the reddened quasars are likely being observed at a younger stage than UV-luminous quasars of similar mass, which have presumably already been through an obscured phase associated with the bulk of their mass assembly.

New large area far-infrared to millimetre surveys such as *Herschel*-ATLAS and surveys with the South Pole Telescope could offer the opportunity to directly detect the host galaxies of this rare population due to surveying much larger areas than covered by previous surveys of the SMG population.

4.3 Obscured fraction of type 1 AGN

We now attempt to derive some constraints on the space density of obscured type 1 AGN in order to address whether these optically obscured sources constitute a significant fraction of the total type 1 AGN population. Previous studies of highly obscured broad-line quasars have relied on matching to radio surveys (e.g. Webster et al. 1995; Glikman et al. 2007) so it is interesting to consider whether similar conclusions about the obscured fraction are reached by studying the more numerous radio-quiet quasars. Obscured, in the context of the following discussion, is taken to mean quasars with $A_V \gtrsim 2$.

In Section 3.1 we fitted model SEDs to the broad-band colours of our reddened quasars in order to infer a dust extinction for each quasar. Using this dust extinction value and our reddening law (Section 3.1), we correct each model SED in order to derive an unreddened SED for each quasar. The left-hand panel of Fig. 10 shows an example of this procedure for our reddest quasar, ULAS J1234+0907. It can immediately be seen that the extinction in the SDSS optical bands is significant; an $A_V = 6.0$ corresponds to an extinction of 17.5 mag at rest frame 2250 Å which makes the quasar undetectable in even deep ground-based optical surveys. Correcting for the extinction makes ULAS J1234+0907 one of the brightest quasars known at these redshifts with an absolute magnitude of $M_i = -31.8$. In Fig. 10 we also plot a model with $A_V = 4.96$ for ULAS J1234+0907 which produces a slightly better match to the spectrum continuum. Adopting this lower extinction value rather than the one inferred from fitting to the broad-band photometry still makes this source a very luminous quasar with $M_i = -31.0$ and does not change our conclusions. In Banerji et al. (in preparation) we present follow-up observations of this source at multiple wavelengths in order to better characterize its nature.

In the right-hand panel of Fig. 10, we plot the extinction-corrected absolute magnitudes versus redshift for all our reddened quasars compared to the SDSS optically selected population of Shen et al. (2011). The total reddened quasar sample from Paper I and this work covers an area of 955 deg^2. We also list these extinction-corrected i-band absolute magnitudes in Table 6. We have used a correction of +0.596 (Richards et al. 2006) to convert between $M_i[z = 2]$ and M_i for the SDSS quasars. The plot illustrates both the reddened absolute magnitudes and the de-reddened absolute magnitudes of our sample in order to demonstrate the effect of extinction on the inferred optical brightness. As can be seen from the figure, the extincted optical magnitudes lie well below the SDSS flux limit for this sample but correcting for this dust extinction makes the reddened quasars as luminous as some of the brightest SDSS sources and, in some cases, brighter than any known SDSS quasar. This is to be expected given that we are selecting red quasars in an NIR flux-limited sample. Consequently, for a constant NIR flux, more heavily obscured sources are going to be more intrinsically luminous. This can be seen in the right-hand panel of Fig. 10 which also shows our K-band selection boundary in the $M_i - z$ plane. Our $(J - K) > 2.5$ colour selection broadly corresponds to selecting quasars at $z \sim 2$ with $E(B - V) \gtrsim 0.5$ (Paper I), albeit with some scatter. We note, however, that while the NIR selection allows us to detect the most heavily obscured intrinsically luminous quasars at $z \sim 2$, it is biased against heavily obscured quasars with more modest luminosities at the same redshifts – i.e. a quasar with $E(B - V) = 1.5$, for example, would have to be one of the most luminous quasars known to make it into our K-band sample at $z \sim 2$. We discuss this selection effect further later in this section.

Fig. 10 clearly demonstrates that the reddened quasars we have found are some of the most intrinsically luminous quasars known at $z \sim 2$. How does their space density compare to the optically selected population? Estimates of the space density of optical quasars

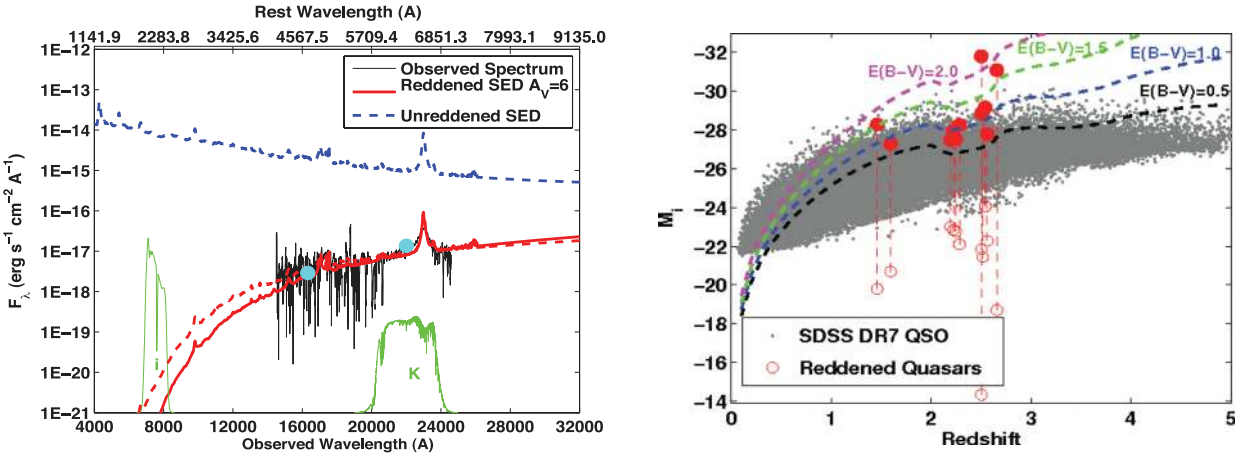

Figure 10. Left: observed VLT-SINFONI spectrum for ULAS J1234+0907 (black) compared to the best-fitting reddened model SED (red) with $A_V = 6.05$ and the unreddened SED (blue) which has been corrected for extinction using the adopted reddening law (Section 3.1). We also plot a model with $A_V = 4.96$ as the red dashed line. This model produces a slightly better match to the spectrum continuum than the $A_V = 6.05$ model fit to the photometry. The UKIDSS H- and K-band fluxes that have been used to derive the higher A_V value are shown as the filled circles. The optical SDSS i-band bandpass and the NIR ULAS K-band bandpass are also shown for reference. ULAS J1234+0907 is a very extreme object with an effective reddening of 17.5 mag in the SDSS i band ($\simeq$2250 Å in the rest frame) making it one of the most intrinsically luminous quasars known. Right: absolute i-band magnitude versus redshift for our reddened quasars compared to the optical quasar population from SDSS DR7. The open circles correspond to the reddened absolute magnitudes and the filled circles represent the extinction-corrected absolute magnitudes with the red dashed lines indicating the effect of extinction for each object. On correcting for the large extinction values, the reddened quasars mostly lie at the most luminous end of the optical sample with no spectroscopically confirmed SDSS quasars that are intrinsically as bright as ULAS J1234+0907 and ULAS J1539+0557. The plot also shows the tracks of a $K = 17$ quasar with different values of $E(B - V)$ in the $M_i - z$ plane corresponding to the flux limit of our survey.

Table 6. De-reddened absolute i-band magnitudes for all our spectroscopically confirmed red quasars. The quasars marked with an asterisk extend to a slightly fainter flux limit of $K_{AB} < 18.9$. They were targeted due to the presence of ancillary multi-wavelength information but do not represent a complete sample and are therefore excluded from the space–density calculations.

Name	Dereddened M_i
ULAS J0016−0038	−27.49
ULAS J0041−0021	−28.94
*ULAS J0141+0101	−27.78
ULAS J0144+0036	−28.26
ULAS J0144−0114	−28.85
ULAS J0221−0019	−27.52
ULAS J1539+0557	−31.08
*ULAS J1002+0137	−27.29
ULAS J1234+0907	−31.81
ULAS J1455+1230	−28.29
ULAS J2200+0056	−29.16
ULAS J2224−0015	−27.96

in the SDSS, for example, are complicated by the fact that the SDSS is highly incomplete in the redshift range $2.2 < z < 2.7$, due to the similarity of Galactic star and quasar colours at these redshifts. Richards et al. (2002, 2006) have, however, studied this incompleteness in detail and corrected for it when deriving the quasar luminosity function. The selection functions derived by these authors were based on comparisons to simulations but have recently been verified empirically using a large sample of KX-selected quasars (Maddox et al. 2012). We can therefore use the SDSS luminosity function to predict the number of UV-bright quasars expected in the redshift range $1.2 < z < 1.75$ or $2.0 < z < 2.7$ over our survey area of 955 deg^2. These numbers of UV-bright quasars should then be directly comparable to the numbers of NIR bright reddened quasars in our sample. We note here that our sample extends to brighter absolute magnitudes than the SDSS but the parametric form of the luminosity function can reasonably be extrapolated to these bright magnitudes in order to provide an estimate for the number of very luminous UV-bright quasars. The completeness-corrected total number of UV-bright quasars at $1.2 < z < 1.75$ or $2.0 < z < 2.7$ over 955 deg^2 of sky predicted from the SDSS luminosity function is given in Table 8.

Our sample of reddened quasars also suffers from incompleteness. The first source of incompleteness arises because not all the red quasar candidates in our UKIDSS sample were targeted for spectroscopy. There are six candidates with colours consistent with identifications as reddened quasars but without spectra. Best-fitting $E(B - V)$ values for these sources are calculated, just as for the spectroscopically confirmed sample, but assuming redshifts of 1.5 and 2.5. Absolute i-band magnitudes can then be calculated as before. The results of this exercise are summarized in Table 7. It can be seen that the absolute i-band magnitudes are similar regardless of the redshift. However, the red $(H - K)$ colours of these sources strongly favour the higher redshift assumption.

The second source of incompleteness is due to morphological misclassification of candidates, whereby some reddened quasars, classified as galaxies in the K band, are not included in our sample. In Paper I we have shown that at the brighter end of our survey the maximum morphological incompleteness in our redshift range is ∼20 per cent.

Finally, as already pointed out in Fig. 10, our flux-limited NIR sample only allows selection of the most intrinsically luminous quasars at $z \sim 2$ with large amounts of dust extinction. More modest luminosity quasars with similar or higher levels of dust obscuration require a deeper K-band survey to be found so we could potentially be missing large numbers of highly reddened quasars at modest luminosities. We estimate our survey incompleteness to a typical $A_V = 2.5$ quasar by assuming that every SDSS quasar at

Table 7. Six quasar candidates for which no spectra were obtained along with their best-fitting $E(B-V)$ values assuming $z = 1.5$ or $z = 2.5$ as well as de-reddened absolute i-band magnitudes corresponding to these two redshifts.

Name	$E(B-V)$, $z=1.5$	M_i, $z=1.5$	$E(B-V)$, $z=2.5$	M_i, $z=2.5$
ULAS J0946+0016	1.38	−28.82	0.80	−28.59
ULAS J1200+0423	1.65	−29.29	0.98	−29.05
ULAS J1320+0948	1.22	−28.36	0.69	−28.12
ULAS J0121+0107	1.06	−28.22	0.60	−28.04
ULAS J0204+0106	1.18	−28.34	0.67	−28.13
ULAS J2346−0038	1.31	−29.62	0.75	−29.38

Table 8. Number of quasars at $1.2 < z < 1.75$ or $2.0 < z < 2.7$ over 955 deg^2 in bins of M_i for our survey of red quasars compared to the SDSS DR7 sample of blue quasars (corrected for completeness). The obscured fraction represents the fraction of reddened quasars relative to the total number of quasars in a particular absolute magnitude bin. In the case of our survey, the lower limits are computed from the raw counts of reddened quasars in this work while the upper limits take into account the various sources of incompleteness in the sample detailed in Section 4.3.

M_i	N/955 deg^2(SDSS DR7)	N/955 deg^2(this work)	Obscured fraction	N/955 deg^2(F2M; Glikman et al. 2007)
−32 to −30	0.36	2–3	80−90 per cent	1
−30 to −29	3.3	1–4	20−60 per cent	0.7
−29 to −28	33	4–17	10−30 per cent	1.8
−28 to −27	304	3–50	1−10 per cent	1

$2.0 < z < 2.5$, for example, has this level of dust extinction, and counting the fraction of these dusty quasars that satisfy our survey selection criteria [$K < 16.5$ and $(J-K) > 2.5$; Vega] in each of the absolute magnitude bins in Table 8. We find that our survey would recover >99 per cent of $A_V = 2.5$ quasars with $-32 < M_i < -30$ at these redshifts with the completeness dropping to ∼90 per cent, 60 per cent and 10 per cent in the subsequent luminosity bins. We correct the numbers of quasars in our survey for all these sources of incompleteness to derive the upper limits quoted in Table 8. These are then compared to the numbers of UV-bright quasars from the SDSS luminosity function over the same redshift range and area to derive an obscured fraction in each absolute magnitude bin.

4.4 Is the obscured fraction luminosity dependent?

Taken at face-value, Table 8 seems to suggest that the obscured fraction of broad-line quasars declines with intrinsic luminosity with these red quasars only making up a relatively small fraction of modest luminosity type 1 quasars at $z \sim 2$. At very high luminosities, however, heavily reddened optically faint quasars dominate the population although with only small numbers at present to exhibit this trend. Is this trend physical or can it simply be explained by selection effects? While it is true that our survey is too bright to detect heavily reddened quasars with $A_V \gtrsim 3$ at $M_i \gtrsim -28$, should large populations of such sources exist, there are several reasons to suggest that this is probably not the case. Flat-spectrum radio-source samples with very high quasar redshift completeness (e.g. Jackson et al. 2002) indicate that the quasar population as a whole cannot consist of a very large fraction of obscured sources (Ellison et al. 2001). Although our sample size is still small, we have carefully taken into account the various selection effects in our survey and we probe down to K-band depths sufficient to detect most $A_V = 2.5$ quasars out to $M_i < -28$ at $z \sim 2$. We conclude that highly reddened quasars are likely to only dominate the counts of type 1 quasars at the brightest absolute magnitudes, where NIR surveys may be more complete than optical surveys.

The above arguments while still tentative due to the small numbers of quasars in our sample seem plausible based on physical arguments. The duty cycle for the obscured phase is likely to be longer for the most luminous quasars, consistent with a longer time required to assemble more massive black holes. Seen another way, the obscured phase is more likely to be associated with the most intrinsically luminous quasars with high-mass accretion rates. These rapidly accreting, massive, obscured black holes should preferentially lie at $z \sim 2$ corresponding to the main epoch of black hole formation. Indeed, our two reddest and most luminous quasars ULAS J1234+0907 and ULAS J1539+0557 lie at the high-redshift end of our sample at $z \sim 2.5$. Our selection criteria do not in any way discriminate against similarly luminous highly reddened quasars at $1.2 < z < 1.75$ but both the quasars observed at these lower redshifts have comparably modest luminosities. Again, we caution against drawing strong conclusions from the very small numbers of sources in our sample but the fact that our most reddened and most luminous quasars are concentrated at the high-redshift end of our sample is also consistent with the most massive black holes assembling the bulk of their mass at early times via an obscured phase.

Taken together, all these facts suggest that the obscured fraction may depend on quasar luminosity with a larger proportion of the most luminous quasars being preferentially observed in an obscured phase at $z \sim 2$. Our sample is still, however, highly incomplete for obscured quasars at $M_i \gtrsim -28$ and a deeper K-band sample is clearly needed to fully test this theory.

4.5 Comparison to the 2MASS sample

Having demonstrated that our population of intrinsically luminous dust-reddened quasars at $z \sim 2$ with $E(B-V) > 0.5$ seem to represent a sizeable fraction of the total quasar population at very bright absolute magnitudes, we now make some explicit comparisons to previous studies of such objects using the shallower ($K_{\rm Vega} < 15$) 2MASS survey (Glikman et al. 2007). Our survey represents a significant increase in depth compared to this previous work and extends 1.5–2 mag fainter in the K band. Isolating only those quasars

in the 2MASS survey that overlap the redshift range of our sample ($1.2 < z < 1.75$ or $2.0 < z < 2.7$), there are only 13 reddened broad-line quasars over 2716 deg^2 in the Glikman et al. (2007) sample. For each of these 13 quasars, we use the K-band magnitudes and dust extinctions given in Glikman et al. (2007) along with the average $(i - K)$ colour of our quasar models (Section 3.1) at that redshift to calculate an absolute i-band magnitude. The counts are then scaled to our survey area of 955 deg^2 and once again quoted in Table 8. Table 8 demonstrates that our NIR selection uncovers much larger numbers of quasars at $z \sim 2$ than Glikman et al. (2007) but with similar intrinsic luminosities and much higher levels of dust reddening. The $z \sim 2$ 2MASS sample has a median $E(B - V) = 0.4$ while our sample over the same redshift range has a median $E(B - V) = 0.8$.

We have also shown that the most heavily dust-reddened quasars in our sample lie at the highest redshifts whereas the reddest quasars in Glikman et al. (2007) are preferentially at the low-redshift end of their sample due to the shallow K-band limit. If red quasars in which the red colours are attributed to dust extinction represent a young phase in quasar evolution, they should preferentially be seen at $z \sim 2$ corresponding to the peak of star formation and black hole accretion. This is what is observed in our sample and suggests that other factors apart from dust extinction in the quasar host may be responsible for the red colours in the reddest quasars in the Glikman et al. (2007) sample. Selecting only quasars with $E(B - V) > 0.5$ from the Glikman et al. (2007) sample in order to overlap the typical reddening in the quasars in our sample, we find a median redshift of 0.6 for these quasars. At these redshifts, the host galaxy contribution to the quasar can be significant, affecting the quasar colours. In addition, at these lower redshifts, the NIR J and K bands are also tracing hot dust emission. In a forthcoming paper, we demonstrate using *WISE* photometry for our quasars that the temperature of this hot dust can significantly affect the colours of quasars at rest-frame wavelengths of 1–2 μm independent of the amount of dust extinction in the quasar host. The advantage of our sample over that of Glikman et al. (2007) is that at the higher redshifts, the hot dust emission is redshifted out of the NIR bands employed for the colour selection so the red colours can more safely be attributed to dust extinction in the quasar host.

5 FUTURE WORK

The current work is based on a sample selected using ∼1000 deg^2 of data from the UKIDSS-LAS. The latest data release of the UKIDSS-LAS spans ∼3600 deg^2. In addition, the ongoing VISTA Hemisphere Survey will provide an additional ∼10 000 deg^2 of high-latitude sky; therefore easily allowing our sample sizes to be increased by an order of magnitude over the next 5 years as well as probing fainter fluxes in the K band. The combination of these NIR surveys with mid-infrared data from the all-sky *WISE* survey will enable statistically significant samples of reddened type 1 AGN to be assembled. We have already embarked on spectroscopic follow-up of these reddened AGN candidates selected from the initial data in the new surveys using Gemini-GNIRS and these new data will allow us to tighten our constraints on the exact obscured fraction of AGN at the main epoch of galaxy assembly and black hole accretion as well as to probe in detail the dependence of this fraction on the quasar luminosity.

6 CONCLUSIONS

We have extended our search for NIR-selected samples of reddened quasars to cover an area of almost 1000 deg^2. Within this area, we have identified a total of 27 very bright K-band sources that also have unusually red colours. 10 of these have been presented in Hawthorn et al. In this paper we present spectroscopic observations of another 13 candidates. Five of these are confirmed to be highly reddened type 1 AGN increasing our total reddened NIR bright AGN sample to 12.

We combine the new sample and the sample from Hawthorn et al. in order to examine the properties of the optically obscured luminous type 1 AGN population. Unlike previous studies, our sample relies on a homogenous selection at NIR wavelengths without needing detections in the optical and/or the radio. We carefully account for the effect of Hα equivalent widths on the infrared colours of our quasars and by probing luminous sources at $z > 1$, eliminate any contribution to their colours from the host galaxy. In particular, we reach to the following conclusions.

(i) Our sample of spectroscopically confirmed reddened quasars with redshifts all possess broad Hα emission indicating that they are canonical type 1 AGN.

(ii) Almost all Hα line profiles are best fitted by a broad ($>5000\,\mathrm{km\,s^{-1}}$) and intermediate ($>1500\,\mathrm{km\,s^{-1}}$) component and some of the lines show significant velocity offsets between the two components indicating the presence of strong outflows in the broad-line region of the AGN. Such outflows are not commonly seen to affect the Hα lines in UV-luminous quasars and provide evidence that the reddened quasars are observed in a phase when they are in the process of expelling their gas and dust.

(iii) We use the broad-band colours to fit model SEDs to all quasars with redshifts and find that significant dust extinction of $A_V = 2$–6 mag is required to fit the observational data making these quasars highly obscured at optical wavelengths. The dust extinctions in our sample are comparable to those seen in the submillimetre galaxy population at similar redshifts and this level of dust obscuration pushes the quasars well below the flux limits of large area optical surveys like the SDSS.

(iv) We use the line profiles to derive virial black hole masses and Eddington fractions for all our reddened quasars. The mean virial black hole mass is $2 \times 10^9\,\mathrm{M_\odot}$ and the mean Eddington fraction is 0.5. The reddened quasars are therefore already as massive as the most massive optically selected quasars but still accreting mass at a relatively high rate. We argue that they probably represent a short-lived phase in quasar evolution when the most massive starbursts are transitioning to UV-luminous quasars.

(v) Two of our confirmed reddened quasars, ULAS J1539+0557 ($z = 2.658$) and ULAS J1234+0907 ($z = 2.503$), are intrinsically brighter than any known SDSS spectroscopic quasars and have mass accretion rates in excess of $100\,\mathrm{M_\odot yr^{-1}}$. They both lie at the high-redshift end of our sample consistent with a picture where the most heavily reddened luminous quasars are accreting the bulk of their mass at early times via an obscured phase.

(vi) We consider the possibility of lensing in our population and conclude that while we cannot rule out the possibility that individual objects are lensed, our sample is generally fainter in the K band than all the known lensed reddened quasars previously found. Crucially, many of our sources are undetected in the SDSS i, z and UKIDSS Y and J bands where a lensing elliptical galaxy at $z \sim 1$ should be visible. The bulk of our reddened quasar population is therefore unlikely to be lensed.

(vii) The broad lines combined with the large dust extinctions observed in our sample strongly point to a specific phase in the quasar life cycle, rather than orientation, being responsible for the red colours. We conclude that our quasars are likely to be observed

in a phase of coeval galaxy and black hole growth when the starburst is decaying but the dust has not yet fully cleared preventing these sources from being selected as optical quasars.

(viii) We use our sample to place new constraints of the fraction of obscured quasars and find tentative evidence that this is a function of intrinsic luminosity and dust reddening. Although a large population of modest luminosity heavily dust-obscured quasars is not ruled out by our data given the *K*-band flux limit of our sample, other independent lines of evidence point to this not being the case. At bright absolute magnitudes however, where we are reasonably complete, the obscured quasars seem to make up a sizeable proportion of the type 1 quasar population suggesting that NIR surveys may be more complete than optical surveys at the very bright-end of the quasar luminosity function at $z \sim 2$.

(ix) The large obscured fractions in the most intrinsically luminous quasars are consistent with these sources having a longer obscured duty cycle. Seen another way, the obscured phase of a quasar is probably likely to be associated with its most intrinsically luminous stage as it corresponds to a time when the black hole is accreting mass very quickly.

(x) Given these results and their possible implications for quasar evolution, a larger sample of *K*-band-selected quasars pushing to fainter *K*-band magnitudes is clearly required to test the hypothesis put forward here that the obscured fraction of type 1 AGN is a function of quasar luminosity.

In conclusion, we have presented a NIR-selected sample of reddened quasars that have been chosen to lie at $1.5 < z < 3$ corresponding to the peak of star formation and black hole accretion in the Universe. Unlike previous studies, we detect populations of quasars that lie well below the SDSS detection limits as well as radio-quiet quasars that are not present in the FIRST radio survey, thus demonstrating the potential of new large area infrared surveys in studying the dust-obscured quasar population. We find that these luminous dusty quasars are likely being observed in a phase of coeval galaxy and black hole growth and are in the process of expelling their gas and dust before turning into UV-luminous quasars. Our ongoing follow-up of these sources at long wavelengths will allow their host galaxy properties to be constrained for the first time.

Having demonstrated the success of NIR surveys in selecting reddened quasars, we have embarked on a spectroscopic campaign to follow-up new sources being discovered in the VISTA Hemisphere Survey and the *WISE*. These new large area data sets will enable much larger samples of dust-obscured quasars to be assembled over the coming years and push to fainter *K*-band limits, thereby allowing accurate constraints to be placed on the physical properties and global space densities of heavily obscured broad-line quasars.

ACKNOWLEDGMENTS

The authors acknowledge the anonymous referee for a very constructive report that helped us improve this manuscript. We thank Gordon Richards for useful discussions and Chris Lidman and Mark Swinbank for their help with preparing the SINFONI IFU observations. MB, PCH and RGM acknowledge support from the STFC-funded Galaxy Formation and Evolution programme at the Institute of Astronomy. SA-Z acknowledges the award of an STFC PhD studentship.

This work is based on observations collected at the European Southern Observatory, Paranal, Chile, (383.A- 0573(A)). This research has made use of the NASA/IPAC Extragalactic Database (NED) which is operated by the Jet Propulsion Laboratory, California Institute of Technology, under contract with the National Aeronautics and Space Administration.

The sky transmission spectrum was created from data that were kindly made available by the NSO/Kitt Peak Observatory. NSO/Kitt Peak FTS data used here were produced by NSF/NOAO.

REFERENCES

Alexander D. M. et al., 2008, AJ, 135, 1968
Allen J. T., Hewett P. C., Maddox N., Richards G. T., Belokurov V., 2011, MNRAS, 410, 860
Annis J. et al., 2011, preprint (arXiv e-prints)
Becker R. H., Gregg M. D., Hook I. M., McMahon R. G., White R. L., Helfand D. J., 1997, ApJ, 479, L93
Becker R. H., White R. L., Gregg M. D., Brotherton M. S., Laurent-Muehleisen S. A., Arav N., 2000, ApJ, 538, 72
Blain A. W., Smail I., Ivison R. J., Kneib J.-P., Frayer D. T., 2002, Phys. Rep., 369, 111
Bonnet H. et al., 2004, The Messenger, 117, 17
Brammer G. B., van Dokkum P. G., Coppi P., 2008, ApJ, 686, 1503
Brusa M. et al., 2010, ApJ, 716, 348
Cannon R. et al., 2006, MNRAS, 372, 425
Coppin K. E. K. et al., 2008, MNRAS, 389, 45
Courbin F., Lidman C., Frye B. L., Magain P., Broadhurst T. J., Pahre M. A., Djorgovski S. G., 1998, ApJ, 499, L119
Cowie L. L. et al., 1994, ApJ, 432, L83
Dey A., Graham J. R., Ivison R. J., Smail I., Wright G. S., Liu M. C., 1999, ApJ, 519, 610
Egami E., Iwamuro F., Maihara T., Oya S., Cowie L. L., 1996, AJ, 112, 73
Eisenhauer F. et al., 2003, in Iye M., Moorwood A. F. M., eds, SPIE Conf. Ser. Vol. 4841, Instrument Design and Performance for Optical/Infrared Ground-Based Telescopes. SPIE, Bellingham, p. 1548
Ellison S. L., Yan L., Hook I. M., Pettini M., Wall J. V., Shaver P., 2001, A&A, 379, 393
Farrah D., Lacy M., Priddey R., Borys C., Afonso J., 2007, ApJ, 662, L59
Farrah D. et al., 2012, ApJ, 745, 178
Gallerani S. et al., 2010, A&A, 523, A85
Glikman E., Helfand D. J., White R. L., Becker R. H., Gregg M. D., Lacy M., 2007, ApJ, 667, 673
Greene J. E., Ho L. C., 2005, ApJ, 630, 122
Gregg M. D., Lacy M., White R. L., Glikman E., Helfand D., Becker R. H., Brotherton M. S., 2002, ApJ, 564, 133
Hall P. B. et al., 2002, ApJS, 141, 267
Helfand D. J., Stone R. P. S., Willman B., White R. L., Becker R. H., Price T., Gregg M. D., McMahon R. G., 2001, AJ, 121, 1872
Hewett P. C., Warren S. J., Leggett S. K., Hodgkin S. T., 2006, MNRAS, 367, 454
Hickox R. C. et al., 2012, MNRAS, 421, 284
Hook I. M., McMahon R. G., Boyle B. J., Irwin M. J., 1994, MNRAS, 268, 305
Hu E. M., Ridgway S. E., 1994, AJ, 107, 1303
Irwin M. J., Ibata R. A., Lewis G. F., Totten E. J., 1998, ApJ, 505, 529
Isaak K. G., Priddey R. S., McMahon R. G., Omont A., Peroux C., Sharp R. G., Withington S., 2002, MNRAS, 329, 149
Jackson C. A., Wall J. V., Shaver P. A., Kellermann K. I., Hook I. M., Hawkins M. R. S., 2002, A&A, 386, 97
Kaspi S., Brandt W. N., Maoz D., Netzer H., Schneider D. P., Shemmer O., 2007, ApJ, 659, 997
Lacy M., Gregg M., Becker R. H., White R. L., Glikman E., Helfand D., Winn J. N., 2002, AJ, 123, 2925
Lawrence A. et al., 2007, MNRAS, 379, 1599
McCracken H. J. et al., 2010, ApJ, 708, 202
McLure R. J., Dunlop J. S., 2004, MNRAS, 352, 1390
Maddox N., Hewett P. C., Warren S. J., Croom S. M., 2008, MNRAS, 386, 1605
Maddox N., Hewett P. C., Peroux C., Nestor D. B., Wisotzki L., 2012, MNRAS, 424, 2876

Mainieri V. et al., 2007, ApJS, 172, 368
Malhotra S., Rhoads J. E., Turner E. L., 1997, MNRAS, 288, 138
Martínez-Sansigre A., Rawlings S., Lacy M., Fadda D., Marleau F. R., Simpson C., Willott C. J., Jarvis M. J., 2005, Nat, 436, 666
Mortlock D. J. et al., 2011, Nat, 474, 616
Ofek E. O., Oguri M., Jackson N., Inada N., Kayo I., 2007, MNRAS, 382, 412
Orellana G., Nagar N. M., Isaak K. G., Priddey R., Maiolino R., McMahon R., Marconi A., Oliva E., 2011, A&A, 531, A128
Priddey R. S., Isaak K. G., McMahon R. G., Omont A., 2003, MNRAS, 339, 1183
Richards G. T. et al., 2002, AJ, 123, 2945
Richards G. T. et al., 2003, AJ, 126, 1131
Richards G. T. et al., 2006, AJ, 131, 2766
Rowan-Robinson M. et al., 1991, Nat, 351, 719
Salvato M. et al., 2009, ApJ, 690, 1250
Sanders D. B., Soifer B. T., Elias J. H., Madore B. F., Matthews K., Neugebauer G., Scoville N. Z., 1988, ApJ, 325, 74
Schneider D. P. et al., 2010, AJ, 139, 2360
Shen Y. et al., 2011, ApJS, 194, 45
Smail I., Ivison R. J., Blain A. W., Kneib J.-P., 2002, MNRAS, 331, 495
Swanson M. E. C., Tegmark M., Hamilton A. J. S., Hill J. C., 2008, MNRAS, 387, 1391
Takata T., Sekiguchi K., Smail I., Chapman S. C., Geach J. E., Swinbank A. M., Blain A., Ivison R. J., 2006, ApJ, 651, 713
Trump J. R. et al., 2009, ApJ, 696, 1195
Urrutia T., Becker R. H., White R. L., Glikman E., Lacy M., Hodge J., Gregg M. D., 2009, ApJ, 698, 1095
Vestergaard M., Peterson B. M., 2006, ApJ, 641, 689
Voit G. M., Weymann R. J., Korista K. T., 1993, ApJ, 413, 95
Warren S. J., Hewett P. C., Foltz C. B., 2000, MNRAS, 312, 827
Watson M. G. et al., 2009, A&A, 493, 339
Webster R. L., Francis P. J., Petersont B. A., Drinkwater M. J., Masci F. J., 1995, Nat, 375, 469
Winn J. N., Lovell J. E. J., Chen H.-W., Fletcher A. B., Hewitt J. N., Patnaik A. R., Schechter P. L., 2002, ApJ, 564, 143
Wright E. L. et al., 2010, AJ, 140, 1868

This paper has been typeset from a TEX/LATEX file prepared by the author.